New Phytologist

Research

Temperature-sensitive male sterility in rice determined by the roles of AGO1d in reproductive phasiRNA biogenesis and function

Chuanlin Shi[1]*, Jie Zhang[2]*, Bingjin Wu[1], Rachel Jouni[3,4], Changxiu Yu[1], Blake C. Meyers[4,5], Wanqi Liang[2] and Qili Fei[1]

[1]Shenzhen Branch, Guangdong Laboratory of Lingnan Modern Agriculture, Genome Analysis Laboratory of the Ministry of Agriculture and Rural Affairs, Agricultural Genomics Institute at Shenzhen, Chinese Academy of Agricultural Sciences, Shenzhen 518120, China; [2]Joint International Research Laboratory of Metabolic and Developmental Sciences, Shanghai Jiao Tong University-University of Adelaide Joint Centre for Agriculture and Health, State Key Laboratory of Hybrid Rice, School of Life Sciences and Biotechnology, Shanghai Jiao Tong University, Shanghai 200240, China; [3]Plant and Microbial Biosciences Program, Division of Biology and Biomedical Sciences, Washington University, Saint Louis, MI 63130, USA; [4]Donald Danforth Plant Science Center, Saint Louis, MI 63132, USA; [5]Division of Plant Sciences and Technology, University of Missouri-Columbia, Columbia, MI 65211, USA

Authors for correspondence:
Qili Fei
Email: feiqili@caas.cn

Wanqi Liang
Email: wqliang@sjtu.edu.cn

Blake C. Meyers
Email: bmeyers@danforthcenter.org

Received: *21 March 2022*
Accepted: *6 August 2022*

New Phytologist (2022)
doi: 10.1111/nph.18446

Key words: anther, Argonaute, microRNA, phasiRNA, rice.

Summary

- Phased secondary siRNAs (phasiRNAs) are broadly present in the reproductive tissues of flowering plants, with spatial–temporal specificity. However, the ARGONAUTE (AGO) proteins associated with phasiRNAs and their miRNA triggers remain elusive.
- Here, through histological and high-throughput sequencing analyses, we show that rice AGO1d, which is specifically expressed in anther wall cells before and during meiosis, associates with both miR2118 and miR2275 to mediate phasiRNA biogenesis.
- AGO1d preferentially binds to miR2118-triggered 21-nucleotide (nt) phasiRNAs with a 5′-terminal uridine, suggesting a dual role in phasiRNA biogenesis and function. Depletion of AGO1d causes a reduction of 21- and 24-nt phasiRNAs and temperature-sensitive male sterility. At lower temperatures, anthers of the *ago1d* mutant predominantly show excessive tapetal cells with little starch accumulation during pollen formation, possibly caused by the dysregulation of cell metabolism.
- These results uncover an essential role of AGO1d in rice anther development at lower temperatures and demonstrate coordinative roles of AGO proteins during reproductive phasiRNA biogenesis and function.

Introduction

Plant small RNAs are key regulators of gene expression at both the post-transcriptional gene silencing (PTGS) level, by mediating mRNA cleavage or translational repression, and at the transcription level, through RNA-directed DNA methylation (RdDM) (Borges & Martienssen, 2015). Among the most well-studied classes of small RNAs, microRNAs (miRNAs), which tend to be 21 or 22-nt in length in plants, play critical roles in regulating plant development, immunity, and abiotic stress responses through PTGS (Li & Zhang, 2016; Song *et al.*, 2019, 2021). A unique function of 22-nt length miRNAs is to generate phased secondary siRNAs (phasiRNAs) from target transcripts by forming RNA-induced silencing complexes (RISCs) with ARGONAUTE1 (AGO1) (Chen *et al.*, 2010; Cuperus *et al.*, 2010; Fei *et al.*, 2018; Yoshikawa *et al.*, 2021). In many angiosperm species, phasiRNAs are generated from noncoding RNAs, such as *TASs*, and protein-coding transcripts, represented by the *nucleotide binding site–leucine-rich repeat* (*NB-LRR*) family (Fei *et al.*, 2013; Liu *et al.*, 2020). It has been widely reported in angiosperms that 22-nt miR2118 and miR2275 trigger the biogenesis of 21- and 24-nt phasiRNAs, respectively, from large numbers of noncoding RNAs with high spatial–temporal specificity across premeiotic and meiotic stages during anther development (Johnson *et al.*, 2009; Song *et al.*, 2012; Zhai *et al.*, 2015; Fei *et al.*, 2016). These reproductive phasiRNAs have been particularly well examined in grasses, and especially in maize and rice, highlighting the essential roles of these two classes of phasiRNAs in male reproductive development in monocots.

Studies of the reproductive phasiRNA pathway in rice have revealed that the biogenesis and function of 21-nt phasiRNAs are important during anther development. Knockout of miR2118, the

*These authors are the co-author and contributed equally to this work.

21-nt phasiRNA trigger, results in defects in anther wall development, with decreased 21-nt phasiRNA abundance (Araki *et al.*, 2020). Notably, 21-nt phasiRNAs with 5′-terminal cytosine (5′ C) preferentially associate with AGO5c, also known as MEIOSIS ARRESTED AT LEPTOTENE1 (MEL1); defects in MEL1 cause early meiotic germ cell arrest and complete sterility (Nonomura *et al.*, 2007; Komiya *et al.*, 2014). Moreover, 21-nt phasiRNAs have recently been reported to maintain meiotic progression by mediating the cleavage of gene transcripts enriched for, but not limited to, carbohydrate biosynthetic and metabolic pathways, and receptor-like kinases in germ cells (Jiang *et al.*, 2020; Zhang *et al.*, 2020). Unlike 21-nt phasiRNAs, which are generated by DICER-LIKE 4 (DCL4) in both monocots and dicots, 24-nt phasiRNAs are generated in grasses by monocot-specific DCL5, which was previously known as DCL3b (Song *et al.*, 2012; Zhang *et al.*, 2015). Mutation of DCL5 in maize results in a loss of 24-nt phasiRNAs and tapetal cell defects, and confers temperature-sensitive male sterility in maize (Teng *et al.*, 2020).

Although much progress has been made in establishing the functions of phasiRNAs during reproductive development, the identity of the specific AGOs which load miR2118 and miR2275 during phasiRNA biogenesis, and whether 21-nt phasiRNAs redundantly associate with AGOs other than MEL1, remain to be determined. Here we show that rice AGO1d preferentially binds to small RNAs with 5′ U, including miR2118 and miR2275, as well as to miR2118-triggered 21-nt phasiRNAs. Depletion of AGO1d causes male sterility at lower temperatures, mainly through defective programmed cell death (PCD) of tapetal cells. Our study thus reveals that AGO1d, which is potentially redundant with other AGO1 paralogues, plays dual roles in phasiRNA biogenesis and function in rice. Furthermore, the lower temperature-sensitive sterile phenotype caused by AGO1d deficiency may be valuable for crop breeding efforts.

Materials and Methods

Plant materials and growth conditions

The rice cultivar Nipponbare (*Oryza sativa* L.) was used in all experiments. Rice plants were grown in paddy fields in Shanghai during summer and in Sanya during winter. For temperature treatment, rice plants grown in the paddy field in Shanghai were transferred to growth chambers when anther development reached stage 3, corresponding to 0.5 cm inflorescences. Temperature treatment was carried out at an average temperature of 22°C for the lower temperature treatment and 28°C for the normal control temperature treatment, at 75% relative humidity under a 12 h : 12 h, light : dark photoperiod until anthesis. After temperature treatment, rice plants were transferred to the paddy field for grain filling.

Real-time quantitative polymerase chain reaction (RT-qPCR) analysis

Total RNA was isolated from plant tissues using TRIzol reagent (Invitrogen). cDNA was synthesized using the HiScript® III 1st Strand cDNA Synthesis Kit with gDNA wiper (Vazyme, Nanjing, China). Quantitative polymerase chain reaction was performed on a 7500 Real-Time PCR System (Applied Biosystems, Foster City, CA, USA) using ChamQ Universal SYBR qPCR Master Mix (Vazyme) with the $2^{-\Delta\Delta Ct}$ method for data analysis. Three biological replicates were performed for the RT-qPCR. The housekeeping gene *UBQ* (*LOC_Os03g13170*) was used as an internal reference to normalize the gene expression.

Plasmid construction and transformation

The CRISPR/Cas9 genome editing construct of rice *AGO1d* was designed as previously reported (Ma *et al.*, 2015), and transformed into the Nipponbare background. Genomic DNA from the transgenic plants was extracted and used as the template for PCR amplification flanking the editing site. Mutations in the transgenic plants were characterized by Sanger sequencing. For *AGO1d* expression vectors, the 2200-bp promoter and full-length coding sequence of *AGO1d* were amplified from Nipponbare cDNA and inserted into the plasmid *pCAMBIA1300-3xFLAG* to generate *pAGO1d::AGO1d-FLAG*. To analyze AGO1d protein localization, the green fluorescent protein (GFP) sequence with a stop codon was amplified and inserted into the *pAGO1d::AGO1d-FLAG* construct to generate *pAGO1d::AGO1d-GFP*. All constructs were transformed into *Agrobacterium tumefaciens* strain EHA105 and introduced into Nipponbare. All primers used in this study are listed in Supporting Information Table S1.

Transient expression and microscopy

To investigate the subcellular localization of all rice AGO1 proteins, full-length coding sequences of *AGO1a*, *AGO1b*, *AGO1c* and *AGO1d* were amplified from the Nipponbare cDNA and inserted into *pCAMBIA1300-35S::GFP* to generate *35S::AGO1s-GFP* constructs. The constructed plasmids were transformed into *A. tumefaciens* strain GV3101 and infiltrated into the young leaves of *Nicotiana benthamiana*. The amplified rice *AGO1* coding sequences were also inserted into the *35S::YFP* plasmid to generate *35S::AGO1s-YFP* constructs and transformed into rice protoplasts prepared from the sheath of 2-wk-old wild-type seedlings using the method described elsewhere (Y. Zhang *et al.*, 2011). The GFP fluorescence signal in tobacco leaf epidermal cells and yellow fluorescent protein (YFP) signal in rice protoplasts were observed using a TCS SP8 laser confocal scanning microscope (Leica, Weztlar, Germany). To observe the fluorescence from the stable line *pAGO1d::AGO1d-GFP*, rice anthers from different developmental stages were dissected and subjected to confocal microscopy.

Histochemical analysis

For chromosome DAPI staining, anthers at stages 7–8 grown in a growth chamber at either 22°C or 28°C were collected and fixed in Carnoy's Fluid. Anthers were squashed on a slide with 1× phosphate buffered saline (PBS) solution (pH 7.4) and then soaked in liquid nitrogen. After removing the coverslips, the

samples were stained with 4′,6-diamidino-2-phenylindole (DAPI) and photographed using an Eclipse Ni-E microscope (Nikon, Tokyo, Japan). For semithin sectioning, anthers of different developmental stages were collected and fixed in FAA solution (50% ethanol, 5% glacial acetic acid and 5% formaldehyde) overnight at 4°C. Then, the samples were dehydrated in a gradient series of ethanol (70%, 90% and 100%) and embedded in Technovit 7100 resin (Hereaus Kulzer, Hanau, Germany), polymerized at 45°C, and sliced into *c.* 2 μm transverse sections using an LKB Ultrotome III (LKB Bromma, Sweden). Sections were then stained with toluidine blue O and photographed using the Eclipse Ni-E microscope.

Immunoprecipitation and small RNA library construction

The expression of FLAG-tagged AGO1d was first confirmed by Western blotting with an anti-FLAG antibody in rice spikelets from *pAGO1d::AGO1d-FLAG* transgenic lines. Three biological replicates of rice spikelets (1.5 g) at developmental stages 4–6, 7–8, and 9 from transgenic plants were collected and ground in liquid nitrogen into fine powder. The ground powder was homogenized in 4 ml extraction buffer (50 mM Tris–HCl pH 7.5, 150 mM NaCl, 0.1% NP-40, 4 mM $MgCl_2$, 5 mM DTT, EDTA-free protease inhibitor cocktail (Roche), and 400 U Rnasin Ribonuclease Inhibitor (Promega)) and centrifuged at 12 000 ***g*** for 10 min. Two hundred microlitres of the supernatant was aliquoted for RNA extraction using TRIzol reagent and used as input for RNA immunoprecipitation sequencing (RIP-seq). The remaining supernatant was precleared with Protein A/G magnetic beads (MedChemExpress, Monmouth Junction, NJ, USA) at 4°C for 1 h and then incubated with the Anti-DDDDK-tag antibody (M185-3 l; MBL, Nagano, Japan) at 4°C for 2 h. Thereafter, 50 μl Protein A/G magnetic beads were added and incubated at 4°C for 1 h. After washing three times with extraction buffer containing 2 mM DTT at 4°C, the magnetic beads were extracted using TRIzol reagent for RNA isolation.

Precipitated RNA was then used for small RNA library construction using the NEBNext Multiplex Small RNA Library Prep Set for Illumina (New England Biolabs, Ipswich, MA, USA). For the RIP-seq input library construction, total RNA was loaded on a 15% urea polyacrylamide gel electrophoresis (PAGE) gel for electrophoresis with the microRNA Marker (New England Biolabs). Small RNA in 15- to 30-nt was extracted from gel slices and used for input library construction. To compare the small RNAs between wild-type and the *ago1d* mutant, anthers at stages 4–6, 7–8, and 9, grown at either 28°C or 22°C were collected, with three biological replicates. The small RNA libraries were prepared from *c.* 2 μg total RNA isolated from each sample using NEBNext Multiplex Small RNA Library Prep Set for Illumina (New England Biolabs). All small RNA libraries were sequenced (single-end 50-bp) on an Illumina NovaSeq 6000 platform at Novogene, China.

Small RNA data analysis

Small RNA sequencing data were preprocessed by removing adapters and then mapped to the *Oryza sativa* v.7.0 genome sequences (MSU Rice Genome Annotation Project) (Kawahara *et al.*, 2013) using Bowtie (Langmead *et al.*, 2009). Small RNA reads mapped to rRNAs were filtered, and the remaining genome-mapped reads were normalized to reads per million reads (RPM). For small RNA annotation, rice noncoding RNA sequences were downloaded from the RNAcentral database (Petrov *et al.*, 2017), miRNA sequences were downloaded from miRBase (Release 22.1) (Kozomara *et al.*, 2019), repetitive genomic sequences were downloaded from the Oryza Repeat Database (Ouyang & Buell, 2004), and *PHAS* loci were obtained from a previous study (Fei *et al.*, 2016). The overall small RNA abundance for each *PHAS* locus was calculated by summing up the normalized abundance of distinct small RNA reads using featureCounts (Liao *et al.*, 2014). Phasing score calculation was performed as described previously (Zhai *et al.*, 2011).

RNA-seq library construction and data analysis

Anthers at stages of 4–6, 7–8, and 9 from both wild-type and mutant rice grown at either 28°C or 22°C were collected with three biological replicates. Total RNA was isolated from each sample and then used for poly(A) RNA isolation with oligo(dT) beads. Poly(A) RNA samples were then used for RNA-seq library construction using the NEBNext Ultra RNA Library Prep Kit for Illumina (New England Biolabs), according to the manufacturer's instructions. RNA-seq libraries were sequenced (paired-end 150-bp) on an Illumina NovaSeq 6000 platform at Novogene, China. After quality control and adapter trimming, reads were mapped to the rice genome sequences using Hisat2 (Kim *et al.*, 2019). Gene expression level quantification and differential expression analysis (q-value < 0.01, FDR < 0.01) were conducted using Cufflinks (Trapnell *et al.*, 2010). Gene ontology enrichment analysis was performed using agriGO v.2.0 (Tian *et al.*, 2017), followed by clustering and visualization using TBtools (Chen *et al.*, 2020).

Mass spectrometry analysis

Anthers at stage 9 from both wild-type and *ago1d* mutant plants grown at either 28°C or 22°C were collected, with three biological replicates. A 50 mg sample of the plant material was taken for liquid chromatography–tandem mass spectrometry (LC-MS/MS) analysis using a UPLC-ESI-MS/MS system (UPLC – Nexera X2; Shimadzu, Tokyo, Japan; MS – 4500 Q-TRAP; Applied Biosystems) at MetWare, China. Significantly differential metabolites between groups were determined by variable importance in projection score (VIP ≥ 1) and absolute log_2FC (|log2FC| ≥ 1; FC, fold change). Variable importance in projection values were extracted from the orthogonal projections to latent structures–discriminant analysis (OPLS-DA) result, which was generated using the R package MetaboAnalystR. In order to avoid overfitting, a permutation test (200 permutations) was performed.

Accession numbers

The gene sequence data for this study can be found in the GenBank/EMBL databases under the following accession numbers:

AGO1a (LOC_Os02g45070), *AGO1b* (LOC_Os04g47870), *AGO1c* (LOC_Os02g58490), *AGO1d* (LOC_Os06g51310) and *UBQ* (LOC_Os03g13170).

Results

Expression specificity and localization of rice AGO1d

The rice *AGO1* gene has four paralogues – *AGO1a*, *AGO1b*, *AGO1c*, and *AGO1d* – a diversification that is conserved in other grasses (Zhang *et al.*, 2015). We previously showed, based on published microarray data, that the expression of *AGO1d* is anther-specific (Fei *et al.*, 2016). Here, we reexamined the expression patterns of all four rice AGO1 paralogues by RT-qPCR. We found that *AGO1a* and *AGO1c* are expressed in all four examined tissues, including root, stem, leaf, and anthers, in different stages (Fig. S1a). Consistent with our previous report (Fei *et al.*, 2016), *AGO1d* shows the highest tissue specificity in rice anthers among the four AGO paralogues, with *c.* 10- to 20-fold higher expression than in vegetative tissues. Similarly, *AGO1b* is expressed in rice anthers at *c.* 3- to 5-fold higher levels than in vegetative tissues (Fig. S1a). These results suggest that *AGO1d* and *AGO1b* may function redundantly during rice anther development.

Arabidopsis AGO1 primarily localizes to the cytoplasm to mediate PTGS (Derrien *et al.*, 2012; Li *et al.*, 2013), although AGO1:miRNA RISC assembly occurs in the nucleus (Bologna *et al.*, 2018), and nuclear-localized AGO1 regulates transcription in response to hormones and stresses (Liu *et al.*, 2018). To examine whether there is divergence in subcellular localization of the rice AGO1 paralogues, we constructed vectors expressing GFP/YFP-tagged rice AGO1 proteins (*35S::AGO1a/b/c/d-GFP/YFP*) and transiently expressed them in both *Nicotiana benthamiana* leaves and rice protoplasts. Confocal fluorescence microscopy revealed that, similar to AGO1 in Arabidopsis, all rice AGO1 proteins predominantly localize to the cytoplasm in tobacco epidermal cells (Fig. S1b) and rice protoplasts (Fig. S1c), suggesting that they may each play a major role in PTGS in rice.

Previous mRNA *in situ* hybridizations showed that *AGO1d* transcripts are highly expressed at earlier stages of anther wall cell development, indicating the functional relevance of this gene, with 21-nt phasiRNAs which peak at premeiotic stages (Fei *et al.*, 2016). Although mRNA expression is generally considered to correlate with protein expression, spatiotemporal discrepancy between mRNA and protein accumulation are sometimes observed due to possible translocation and higher stability of proteins. To determine if the expression pattern of AGO1d protein remains consistent with its mRNA, we generated AGO1d-GFP transgenic lines using its native promoter (*pAGO1d::AGO1d-GFP*), and observed the GFP signal at different anther developmental stages as described previously (D. Zhang *et al.*, 2011). We observed an intense GFP signal in all layers of the anther wall cells across stages 5 to 8a, followed by a reduction in fluorescence intensity in the epidermis and tapetum at stages 8a to 9 (Fig. 1), temporally overlapping with both 21- and 24-nt phasiRNA biogenesis. Consistent with the transient expression results, AGO1d-GFP mainly accumulates in the cytoplasm of anther wall cells (Fig. 1). During rice microsporogenesis, microspore mother cells (MMCs) undergo meiosis I from stages 7 to 8a, and meiosis II from stages 8a to 8b, and free haploid microspores are released from tetrads at stage 9 (D. Zhang *et al.*, 2011). Therefore, AGO1d protein is expressed in all layers of anther wall cells with its highest accumulation before and during meiosis, suggesting the possibility of a functional role in 21- and 24-nt phasiRNA biogenesis.

AGO1d depletion confers temperature-sensitive male sterility in rice

To investigate the function of AGO1d in rice microsporogenesis, CRISPR/Cas9 vectors were constructed and transformed into rice (*Oryza sativa* L. *japonica* cv. Nipponbare) to knock out AGO1d. The guide RNA was designed to target the 5′ end of the first exon of *AGO1d* to attain null mutant lines (Fig. 2a). A total of seven lines were confirmed to have shifted open reading frames, as determined by Sanger sequencing (Fig. 2a). However, *ago1d* null mutants displayed anther morphology and male fertility indistinguishable from that of wild-type under normal growth conditions (Fig. S2a,b), suggesting that AGO1d is dispensable for anther development under normal growth conditions. Surprisingly, we observed a >80% reduction in seed setting in mutant *ago1d* lines when grown in a paddy field in winter in Sanya, Hainan Province, China (Fig. S2c). Considering the average temperature can drop as low as *c.* 20°C during anther development (Fig. S2d), we speculated that the lower temperature might underlie male sterility in the winter field-grown *ago1d* mutants.

To test this hypothesis, when panicles of wild-type and *ago1d* mutant rice plants grown in a paddy field reached 0.5 cm in length, the plants were transferred to one of two glasshouses, one of which had an average temperature of 28°C, and the other, 22°C (Fig. S2e). There were no obvious differences in anther morphology, pollen fertility, or plant architecture between wild-type and *ago1d* mutants under 28°C growth conditions (Fig. 2b–d). Interestingly, we found that anthers from *ago1d* mutants, but not wild-type plants, were white and lacked viable pollen grains when grown at 22°C (Fig. 2e,f). The *ago1d* plants grown at 22°C also show no obvious architectural differences (Fig. 2g), but their panicles had significantly lower seed setting percentages compared with wild-type plants grown at 22°C and *ago1d* mutants grown at 28°C, both of which had normal seed setting percentages (Fig. 2h–j). Additional *ago1d* mutant lines under the lower temperature treatment also exhibited a substantial reduction in viable pollen (Fig. S2f) and seed setting (Fig. S2g,h). We used the mutant line *ago1d* #1 for the analyses discussed hereafter, unless otherwise specified. To further investigate the developmental defects in *ago1d* mutant anthers, we performed cytological analysis using anther cross-sections at different developmental stages grown at either 28°C or 22°C. The *ago1d* mutant grown at 22°C showed similar cytological features to other lines during premeiotic stages (S6 to S7), meiotic stages (S8a,b), and the microspore release stage (S9) (Fig. 2k). However, at stage 10, an excessively deformed tapetum was observed in the

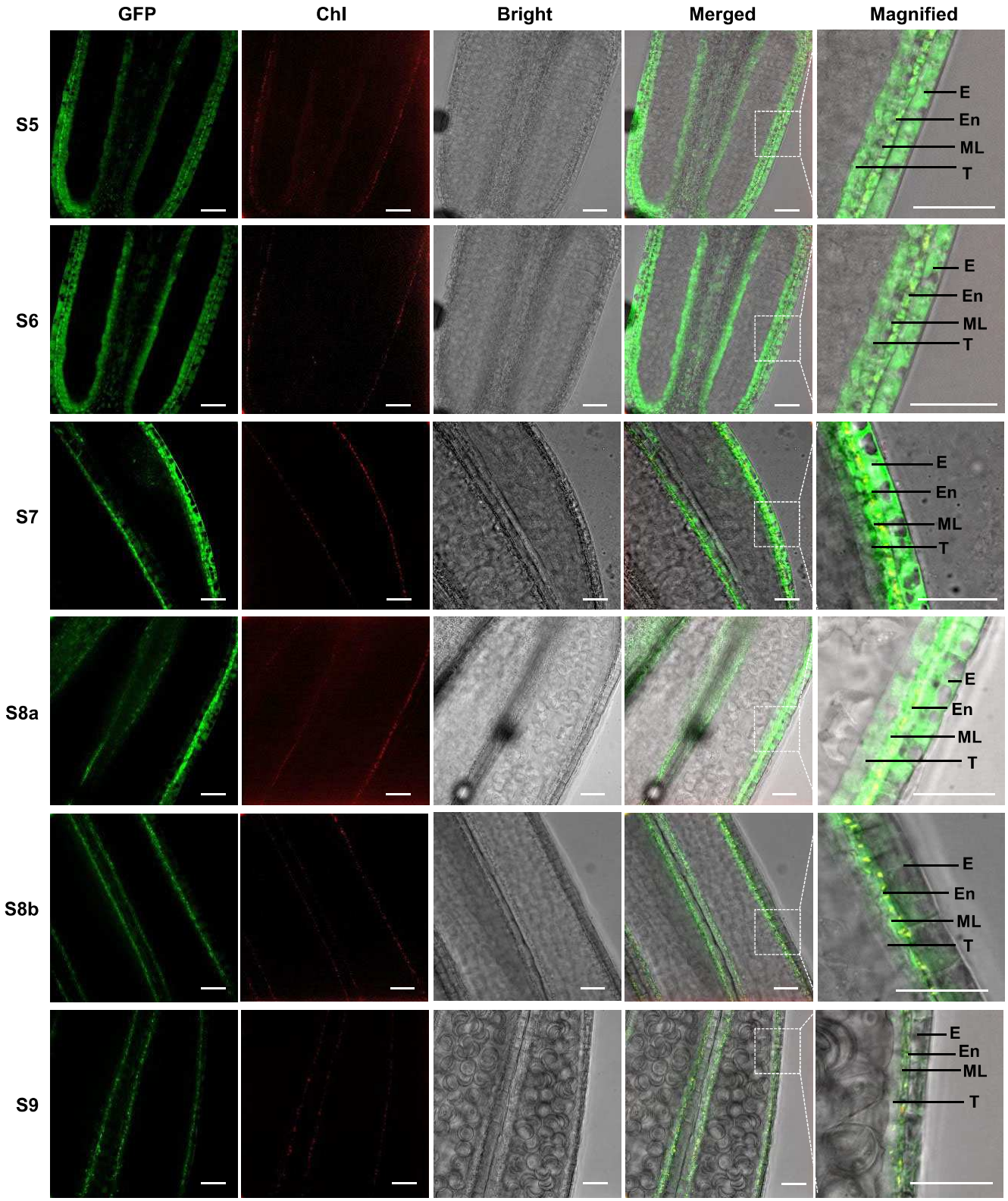

Fig. 1 Expression specificity of AGO1d in rice anthers. Confocal microscopy of the transgenic *pAGO1d::AGO1d-GFP* line. Anthers at different developmental stages were collected, and are labeled along the left side of the figure from stage 5 (S5) to stage 9 (S9). E, epidermis; En, endothecium; ML, middle layer; T, tapetum. Bar, 50 μm.

ago1d mutant locules ($n = 80$) at 22°C (Fig. S2i), possibly due to defective PCD, while the other three lines initiated tapetal degeneration with normal vacuolation (Fig. 2k). Thereafter, the *ago1d* anther at 22°C started to form defective bicellular pollen at stage 11, with little starch accumulation, and failed to produce mature pollen at stage 12 (Fig. 2k).

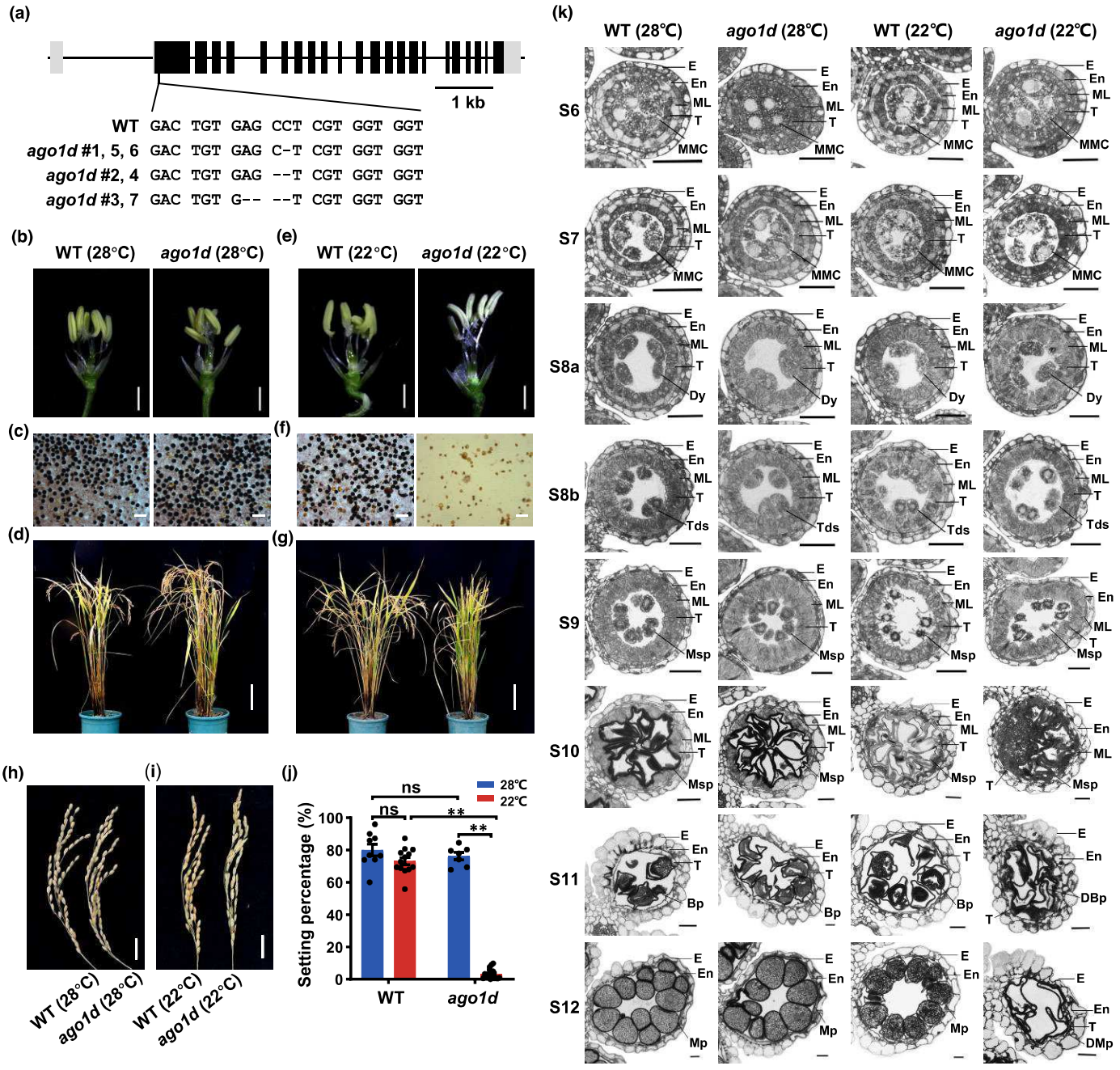

Fig. 2 Temperature-sensitive male fertility phenotypes of the *ago1d* mutant rice plants. (a) Scheme representation of CRISPR/Cas9 target sites on the *AGO1d* gene. Mutations for each line are indicated below the gene model. (b, e) Anthers at stage 13 of the wild-type (WT) and *ago1d* knockout line #1 grown at 28°C (b) and 22°C (e). Bar, 1 mm. Sample labels above panels (b, e) also apply to panels (c, d, f, g). (c, f) Stained pollen from wild-type (WT) and *ago1d* knockout line #1 grown at 28°C (c) and 22°C (f) with iodine potassium iodide (I_2-KI) solution. Bar, 200 μm. (d, g) Whole rice plants of wild-type (WT) and *ago1d* knockout line #1 grown at 28°C (d) and 22°C (g) after heading. Bar, 10 cm. (h, i) Seeded panicles of wild-type and *ago1d* #1 at 28°C (h) and 22°C (i). Bar, 2 cm. (j) Seed setting percentages ($n \geq 7$; three panicles from each plant were counted). Values are given as the mean ± SEM. Asterisks indicate significant differences according to Student's *t*-test. (**, $P < 0.01$ and ns, not significant). (k) Semithin sections of anthers from stage 6 to stage 12 from wild-type and *ago1d* #1 plants grown at 28°C and 22°C. Bp, bicellular pollen; DBp, defective bicellular pollen; DMp, defective mature pollen; Dy, dyad cell; E, epidermis; En, endothecium; ML, middle layer; MMC, microspore mother cell; Mp, mature pollen; Msp, microspore; T, tapetum; Tds, tetrads. Bar, 25 μm.

In addition to cytological analysis, we analyzed meiotic chromosome behavior using DAPI-stained male meiocytes to compare meiotic progression in wild-type and *ago1d* mutants grown at 22°C. Among the 392 *ago1d* meiocytes we examined, 95.6% (375/392) showed normal meiotic progression (Fig. S3a), compared with 98.3% (341/347) in the wild-type, suggesting

slightly higher meiotic defects in the *ago1d* mutant grown at lower temperatures. Univalent or randomly distributed chromosomes and chromosome bridges were found among the abnormal events in both the wild-type (1.7%) and mutant (3.1%) plants (Fig. S3b). However, aberrantly decondensed chromosomes (1.3%) were only observed in the *ago1d* mutant (Fig. S3b), a phenotype reminiscent of the *eternal tapetum 1* (*eat1*) mutant. EAT1 is a transcription factor that mediates the transcription of 24-nt phasiRNA precursors (Ono *et al.*, 2018), suggesting functional connections between AGO1d and 24-nt phasiRNAs. Taken together, *ago1d* loss-of-function predominantly causes defective tapetal cell PCD during pollen formation and mildly affects meiosis, resulting in male sterility and a dramatic decrease in seed setting percentages at lower temperatures.

Rice AGO1d preferentially loads small RNAs with 5′ U, including miRNAs and 21-nt phasiRNAs

Specificity for small RNAs with 5′ U has been reported for AGO1a, AGO1b, and AGO1c (Wu *et al.*, 2009). Due to the degree of sequence similarity observed, we reasoned that AGO1d may also preferentially load small RNAs with 5′ U. To investigate this, we generated AGO1d-FLAG transgenic lines using its native promoter (*pAGO1d::AGO1d-FLAG*). Western blotting using an anti-FLAG antibody confirmed the successful expression of FLAG-tagged AGO1d with two clear bands (Fig. S4a), which may be derived from alternative splicing of *AGO1d* transcripts. We next performed immunoprecipitation of AGO1d using rice spikelets at three different developmental stages and constructed small RNA libraries from the immunoprecipitated RNAs for high-throughput sequencing (RIP-seq). We found that the percentage of 24-nt small RNAs was diminished relative to 21-nt small RNAs in all RIP samples (Fig. S4b,c), suggesting that AGO1d disfavors 24-nt small RNAs.

We focused on analyzing a few categories of small RNAs, including miRNAs, 21- and 24-nt reproductive phasiRNAs, 24-nt repeat-associated siRNAs (rasiRNAs), and other 21-nt siRNAs, because of their functional significance in plants. By comparing their abundances between RIP and input samples, we found that the majority of 5′ U, but not 5′ A/C/G miRNAs (Fig. 3a–d; Dataset S1), 21-nt phasiRNAs (Fig. 3e–h), and other 21-nt siRNAs (Fig. S5a) are enriched in RIP samples at all stages. Accordingly, their overall abundances are consistently higher in the RIP samples (Figs 3b,d,f,h, S5a). Thus, in addition to MEL1, which is known to favor 21-nt phasiRNAs with 5′ C in germ cells, we have discovered that AGO1d tends to load 21-nt phasiRNAs with 5′ U in anther wall cells. By contrast, neither 24-nt phasiRNAs nor 24-nt rasiRNAs were enriched in the RIP samples, regardless of the 5′ nucleotide (Fig. S5b,c), confirming that 24-nt small RNAs are not favored by AGO1d. In summary, we have shown that AGO1d preferentially associates with 21-nt small RNAs with 5′ U, including miRNAs and 21-nt phasiRNAs.

miR2118 and miR2275 associate with AGO1d to mediate phasiRNA biogenesis

We next investigated whether miR2118 or miR2275 were enriched in the AGO1d RIP-seq samples, because their effector AGO proteins remain unknown. The miR2118 family in rice contains *c.* 18 members that produce 12 distinct mature miR2118 sequences, the vast majority of which contain 5′ U (Araki *et al.*, 2020). We found that most miR2118 members are indeed enriched in the AGO1d RIP samples compared with the input (Fig. 4a; Table S2). Considering that there are only four miR2275 records (miR2275a/b/c/d) in miRBase (Release 22.1), we speculated that more copies of miR2275 may exist in the rice genome. A BLASTN search against the rice genome (MSU7) using these four precursor sequences identified a total of 12 miR2275 members, processed into 10 distinct sequences of mature miR2275 (Table S3). Similar to miR2118, miR2275 members are also enriched in the RIP samples (Fig. 4b; Table S4), including those (miR2275d/e/j/l) with 5′ C. These results suggests that AGO1d also associates with a set of small RNAs with 5′ C, despite a preference for 5′ U. Collectively, both miR2118 and miR2275 were loaded into AGO1d, probably mediating reproductive phasiRNA biogenesis.

To confirm this, we prepared small RNA libraries from three developmental stages of rice anthers from both wild-type and *ago1d* mutants grown at 28°C or 22°C. By comparing the total abundances of phasiRNAs from characterized loci that generate 21- and 24-nt phasiRNAs (21-*PHAS* and 24-*PHAS* loci) (Fei *et al.*, 2016), we found that the overall phasiRNA abundances from most *PHAS* loci are reduced in the mutant compared with wild-type plants, regardless of the growth temperature (Fig. 4c,d; Dataset S2), and the reduction of phasiRNAs from 21- and 24-*PHAS* loci are statistically significant in the *ago1d* mutant at most stages and conditions (Fig. S6a). By contrast, miRNA abundances did not show any significant difference between wild-type and *ago1d* plants at either growth temperature (Fig. S6b; Dataset S3). Genome browser views of randomly selected 21- or 24-*PHAS* loci consistently showed that both classes of phasiRNAs are dramatically decreased in the mutant, consistent with a reduction of phasing scores (Fig. 4e). Taken together, these results confirm that AGO1d mediates 21- and 24-nt reproductive phasiRNA biogenesis through formation of RISCs with miR2118 and miR2275, respectively.

Metabolic dysregulation in *ago1d* anthers at lower temperatures

To investigate gene expression changes underlying temperature-sensitive sterility in the *ago1d* mutant, we performed transcriptome profiling of the anthers of wild-type and *ago1d* plants, grown at 28°C or 22°C, at various developmental stages. We found that *AGO1d* expression was diminished in the *ago1d* mutant anthers (Fig. S7a), possibly due to nonsense-mediated RNA decay triggered by premature translational termination. *AGO1a/b/c* were not upregulated in the *ago1d* mutant

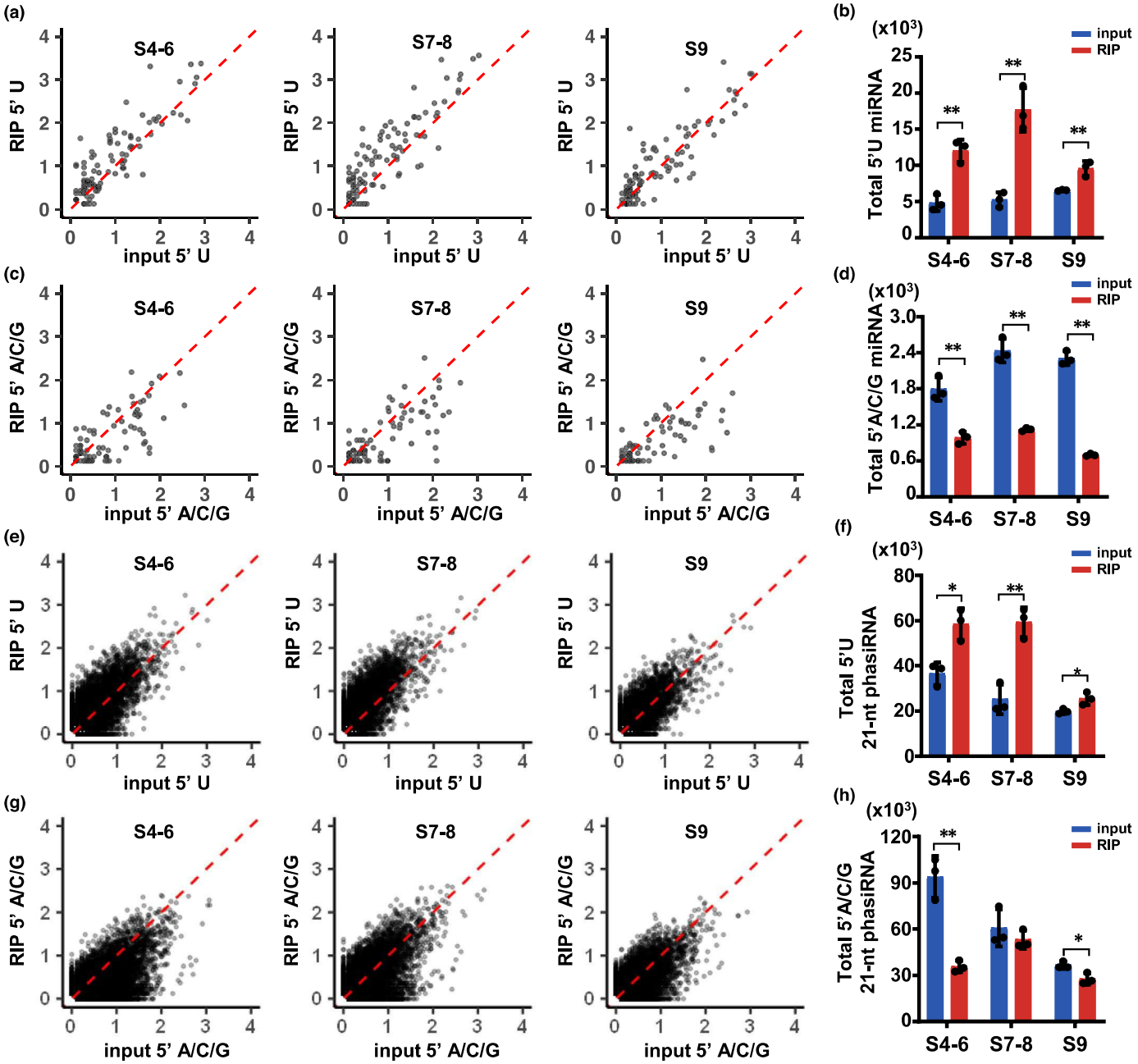

Fig. 3 Enrichment of miRNAs and 21-nt phasiRNAs in rice anthers in the AGO1d-FLAG RIP-seq data. (a) Scatter plots of the abundances (log_{10}RPM) of miRNAs with 5′-terminal uridine (5′ U) in the RNA immunoprecipitation (RIP) samples (*y*-axis) compared with those in the input samples (*x*-axis). Sample stages are labeled on each plot. (b) Comparisons of total 5′ U miRNA abundances between RIP and input at three stages of anther development ($n = 3$ replicates). (c) Scatter plots of the abundances (log_{10}RPM) of miRNAs with 5′-terminal adenine, cytosine, or guanine (5′ A/C/G). Sample stages are labeled on each plot. (d) Comparisons of total 5′ A/C/G miRNA abundances ($n = 3$ replicates). (e) Scatter plots of the abundances (log_{10}RPM) of 21-nt phasiRNAs with 5′ U in the RIP samples (*y*-axis) compared with those in the input samples (*x*-axis). Sample stages are labeled on each plot. (f) Comparisons of total 5′ U 21-nt phasiRNAs abundances ($n = 3$ replicates). (g) Scatter plots of the abundances (log_{10}RPM) of 21-nt phasiRNAs with 5′ A/C/G. Sample stages are labeled on each plot. (h) Comparisons of total 5′ A/C/G 21-nt phasiRNAs abundances ($n = 3$ replicates). Values are given as the mean ± SD. Asterisks indicate significant differences according to Student's *t*-test (*, $P < 0.05$; **, $P < 0.01$).

(Fig. S7b–d), suggesting that there is no compensation at the transcriptional level among the *AGO1* paralogues. Using pairwise differential gene expression analysis for the *ago1d* mutant at 22°C and all other groups, including *ago1d* at 28°C, wild-type at 28°C, and wild-type at 22°C, we aimed to identify key genes and pathways that may underlie sterility in the *ago1d* mutant at lower temperatures. A total of 109, 286, and 273 overlapped differentially expressed genes (DEGs) from stages 4–6, stages 7–8, and stage 9 were identified, respectively (Fig. 5a,b; Dataset S4). A number of genes with well-characterized functions in the regulation of rice anther development and male sterility were identified as DEGs (Fig. S8). Gene ontology (GO) analysis showed that

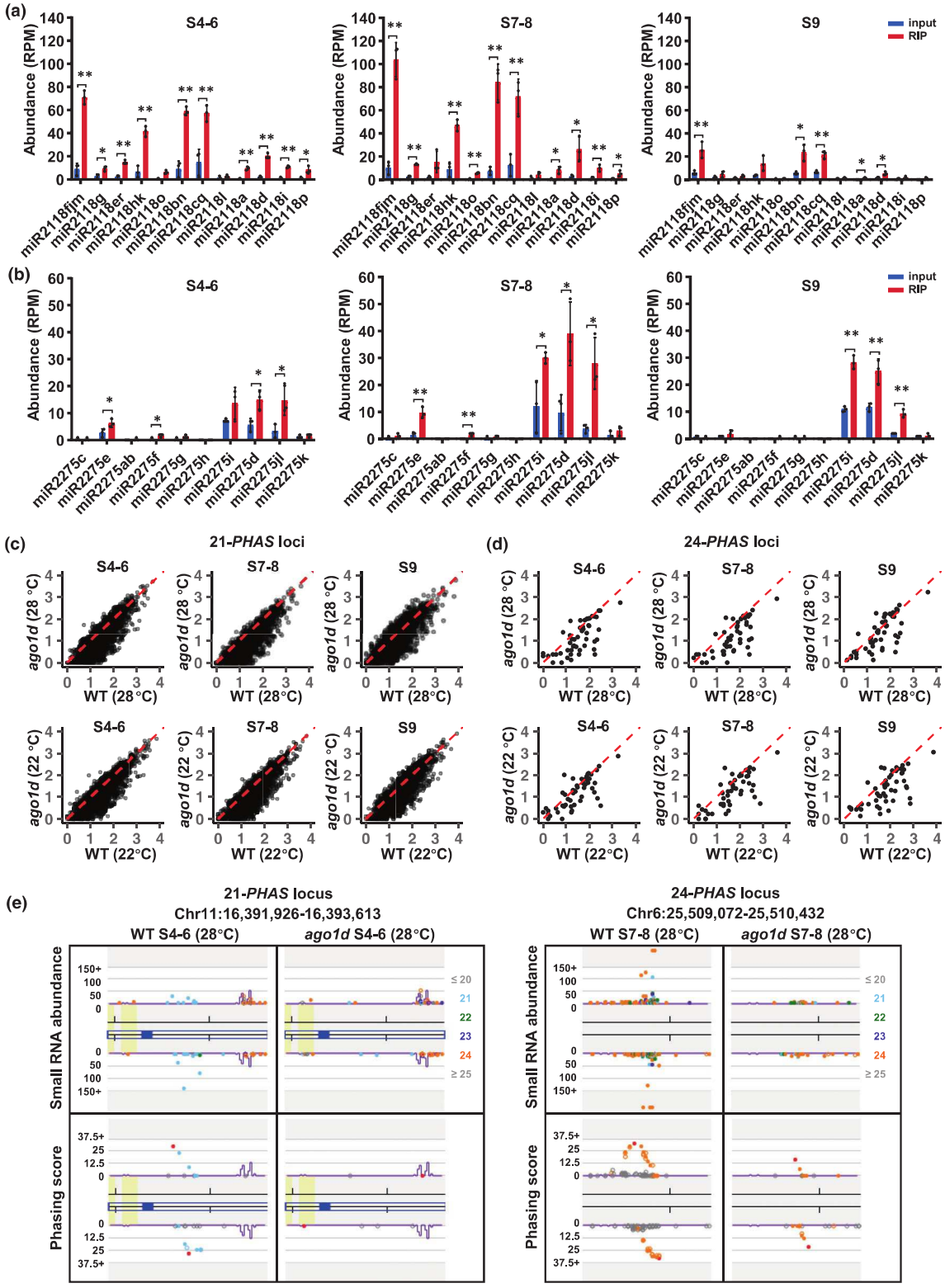

Fig. 4 miR2118 and miR2275 associate with AGO1d to generate phasiRNAs in rice anthers. (a, b) Abundances reads per million (RPM) of different members of miR2118 (a) and miR2275 (b) in the RNA immunoprecipitation (RIP-seq) data. Values are given as the mean ± SD and indicate the average normalized abundances from three biological replicates of small RNA libraries. Asterisks indicate significant differences according to Student's *t*-test (*, $P < 0.05$; **, $P < 0.01$). Sample stages are labeled at the top of each bar graph. (c, d) Scatter plots of the small-RNA abundances (log_{10}RPM) from 21-nt (c) and 24-nt (d) *PHAS* loci in wild-type (WT) and *ago1d* mutant plants grown at 28°C or 22°C. (e) Genome browser views of small RNA distributions from randomly selected 21- and 24-nt *PHAS* loci (upper panels). The *y*-axis represents the abundance (RP3M) of small RNAs. Genomic coordinates and anther stages are indicated at the top of each panel. Small RNAs in different sizes are indicated using different colors. Lower panels show phasing scores of each locus using a sliding window; red dots indicate the highest score at each *PHAS* locus.

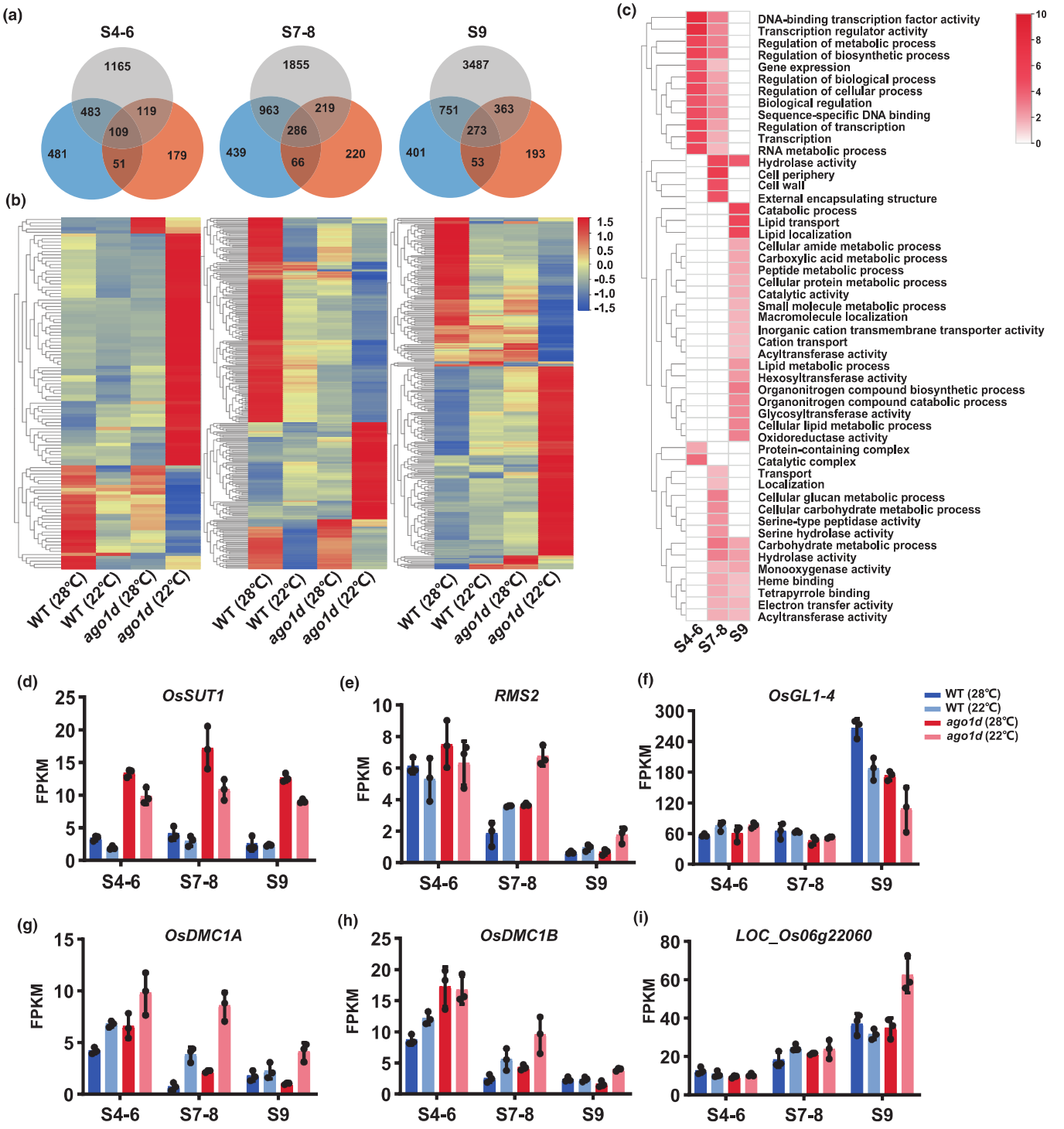

Fig. 5 Transcriptome analysis of wild-type (WT) and *ago1d* rice anthers at grown at 28°C or 22°C. (a) Venn diagrams showing the overlapped DEGs of *ago1d* at 22°C compared with wild-type (WT) plants grown at 28°C (top), WT plants grown at 22°C (right) and *ago1d* plants grown at 28°C (left), respectively, at three anther developmental stages. (b) Heatmap showing the relative expression of 109, 286, and 273 overlapped DEGs at stages corresponding to those shown in (a). Values are scaled by row. (c) Gene ontology enrichment analysis of the overlapped DEGs. The colored scale indicates the *P*-value ($-\log_{10}$) of enriched GO terms. (d–i) Expression levels (in fragments per kilobase of transcript per million mapped reads (FPKM)) of genes regulating anther development from the overlapped DEGs. Values are given as the mean ± SD and indicate the average FPKM values from three biological replicates of RNA-seq libraries.

transcription factor activity was among the most significantly enriched GO terms during stages 4–6, which remained outstanding until stages 7–8; GO terms related to hydrolase activity, cell wall, and carbohydrate metabolism were highly enriched during stages 7–8; GO terms related to catabolic processes and lipid transport, localization, and metabolism were enriched at stage 9

(Fig. 5c). Overall, distinctive transitions during anther development – from transcriptional regulation to carbohydrate metabolism, and then to lipid regulation – were identified for DEGs, which may be perturbed in *ago1d* at lower temperatures and result in anther sterility.

Sugar and lipid metabolism has been extensively shown to play pivotal roles in tapetum development and pollen formation (Wan *et al.*, 2020; Liu *et al.*, 2021). Indeed, alteration of expression levels was observed for many genes involved in carbohydrate metabolic processes and glycosyltransferase activity (Fig. S9), lipid transport, localization, and metabolism (Fig. S10). In particular, *OsSUT1*, which encodes a sucrose transporter (Hirose *et al.*, 2010), was upregulated at stage 9 in *ago1d* plants grown at 28°C and those grown at 22°C (Fig. 5d). In addition, *RMS2*, which encodes a GDSL lipase (Zhao *et al.*, 2020), and *OsGL1-4*, regulators of wax synthesis (Yu *et al.*, 2019), were differentially upregulated and downregulated at stages 7–8 and stage 9 (Fig. 5e,f).

We next performed mass spectrometry analysis of anthers at stage 9 to identify dysregulated metabolites in carbohydrates, lipids, and other metabolic products such as organic acids, amino acids and nucleotide derivatives in the *ago1d* mutant (Fig. S11a,e; Dataset S5). While some of the essential metabolites, such as D-sucrose, D-glucose and D-fructose, remained unchanged, a number of important carbohydrate and lipid metabolites, such as UDP-glucose, D-fructose-1,6-biphosphate, Lyso-phosphatidylethanolamine (LysoPE), α- and γ-linolenic acid, were significantly up- or down-regulated in the *ago1d* mutant at 22°C (Fig. S11f–o). These findings indicate that metabolism is partially disrupted in the *ago1d* mutant at lower temperatures, possibly as a result of transcriptomic changes.

Gene expression regulation by 21-nt phasiRNAs

We next asked whether these dysregulated genes are targets of 21-nt phasiRNAs. Previous studies identified 2281 and 506 targets of 21-nt phasiRNA in rice anthers (Zhang *et al.*, 2020) and meiocytes (Jiang *et al.*, 2020), respectively, by degradome sequencing. Of a total of 608 DEGs identified in *ago1d* plants grown at 22°C in our study, 57 were identified as 21-nt phasiRNA targets in previous studies (Fig. S12a). Among the 57 genes, 22 were upregulated in at least one stage in *ago1d* at 22°C (Fig. S12b), possibly due to the downregulation of 21-nt phasiRNAs. We reason that the downregulation of genes might be due to either indirect effects in the mutant or the low confidence of target identification, considering there were only 88 common targets from these two independent studies. Jiang *et al.* (2020) identified 71 transposable elements (TEs) as phasiRNA targets, expression of only 33 TEs was detected in our RNA-seq data and none of these were significantly differentially expressed in *ago1d* at 22°C (Fig. S12c).

Among the 22 upregulated target genes, *OsDMC1A* was previously validated as a target of two individual 21-nt phasiRNAs (Jiang *et al.*, 2020; Zhang *et al.*, 2020) (Fig. S12d). Although the *ago1d* mutation had limited defects in meiosis, *OsDMC1A* and *OsDMC1B*, which encode meiosis-specific DNA recombinases that redundantly regulate synapsis during meiosis (Wang *et al.*, 2016), were upregulated at almost all stages in *ago1d* anthers grown at 22°C (Fig. 5g,h). Further supporting the upregulation of *OsDMC1A*, the phasiRNA '21PHAS1857_165(+)' targeting it was observed to be downregulated in the *ago1d* mutant, while the other, '21 nt:1:seq-2926', remained at a very low level (Fig. S12d). Neither of these phasiRNAs were enriched in AGO1d RIP-seq data, suggesting that they might be loaded into other AGOs for gene silencing. Interestingly, *LOC_Os06g22060*, which encodes a pyrophosphate:fructose-6-phosphate 1-phosphotransferse (PFP) subunit alpha that is responsible for D-fructose1,6-bisphosphate synthesis (Plaxton, 1996; Lim *et al.*, 2009), was reported as a target of the 21-nt phasiRNA '21 nt:1:seq-38 043' (Zhang *et al.*, 2020). Consistent with the upregulation of this gene (Fig. 5i), the corresponding phasiRNA was downregulated in the *ago1d* mutant (Fig. S12e). AGO1d RIP-seq revealed that this phasiRNA can also associate with AGO1d. Moreover, mass spectrometry analysis found that the product of this gene, D-fructose-1,6-bisphosphate, was also overaccumulated in *ago1d* at 22°C (Fig. S11j). D-fructose-1,6-bisphosphate is an intermediate in the glycolytic pathway, suggesting a direct regulation of sugar metabolism by a 21-nt phasiRNA. Considering the limited number of validated phasiRNA targets, the development of approaches for more precise target identification, in combination with in-depth functional studies in the future, would better demonstrate the roles of phasiRNAs in metabolic regulation during reproduction.

Discussion

AGO proteins are key effectors that regulate gene expression by forming RISCs with small RNAs. The AGO gene family experienced intensive diversification during plant evolution (Zhang *et al.*, 2015). In plants, AGO1 is the major AGO to associate with miRNAs for PTGS. In maize and rice, *AGO1* has expanded into four paralogues: *AGO1a*, *AGO1b*, *AGO1c*, and *AGO1d*. We show that AGO1d has evolved with expression specificity in rice anthers. Despite their diverged tissue specificity, all rice AGO1 proteins predominantly localize to the cytoplasm, similar to the AGO1 orthologue in Arabidopsis, suggesting a consistent function in PTGS. It has been shown by mRNA *in situ* hybridization that *AGO1d* mRNA is expressed in rice anther wall cells, but whether AGO1d protein remains in the same cell types was unclear. Here we demonstrate that AGO1d protein accumulates in all layers of anther wall cells, but not germline cells, across premeiotic and meiotic stages. We previously speculated that AGO1d might be functionally relevant to phasiRNAs, due to its spatiotemporal co-expression with miR2118 and temporal co-expression with *MEL1* (Fei *et al.*, 2016). In addition, a study of maize anthers showed that miR2118 is expressed in the epidermal cells at premeiotic stages, while miR2275 accumulates mainly in tapetal and germ cells during meiosis (Zhai *et al.*, 2015). Therefore, AGO1d protein expression spatiotemporally overlaps with miR2118 and miR2275 (Fig. 6a), supporting the notion that AGO1d may take part in the reproductive phasiRNA pathway during microsporogenesis.

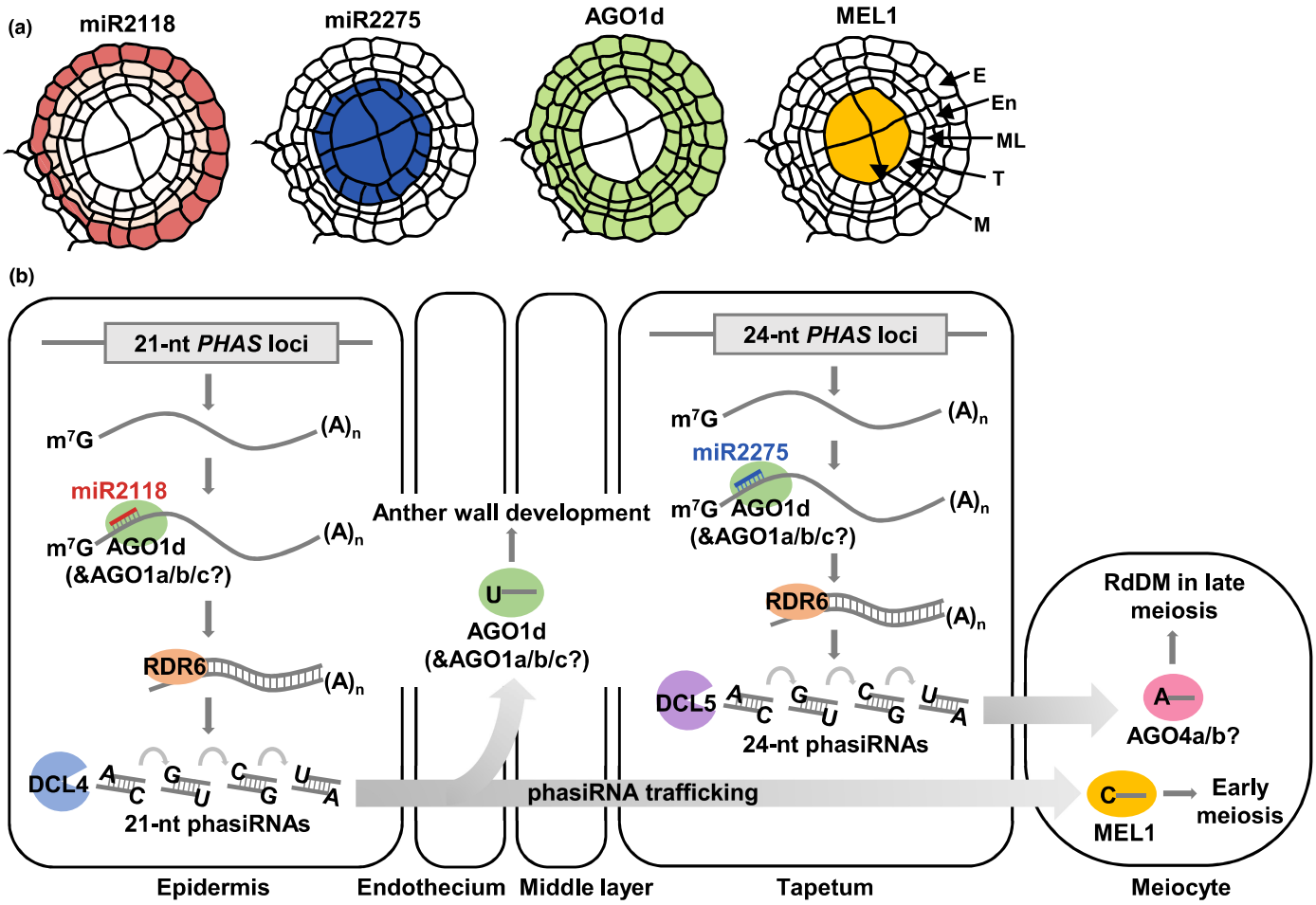

Fig. 6 A proposed model of phasiRNA biogenesis and function in rice anthers. (a) Schematic representation of the expression specificity of miR2118 (red), miR2275 (blue), AGO1d (green), and MEL1 (yellow) in rice anther cells. Each layer of cells is specified by an arrow: E, epidermis; En, endothecium; ML, middle layer; T, tapetum; M, meiocyte. (b) Biogenesis, localization, and function of phasiRNAs in different cell types. AGO1d, potentially redundantly with AGO1a/b/c, binds to miR2118 and miR2275 in the epidermis and tapetum to generate 21- and 24-nt phasiRNAs, respectively. The 21-nt phasiRNAs with 5′ U can spread to all layers of anther wall cells by trafficking and can be loaded to AGO1d, and possibly AGO1a/b/c, to regulate anther wall development. The 21-nt phasiRNAs with 5′ C move to the meiocyte and associate with MEL1 to regulate gene expression during early meiosis. The 24-nt phasiRNAs can transport from the tapetum to meiocytes during late meiosis to mediate DNA methylation, possibly by associating with AGO4a/b, which might prefer 5′ A, as in Arabidopsis.

Surprisingly, when grown under normal growth conditions, *ago1d* null mutants generated by CRISPR/Cas9-mediated genome editing showed no discernable developmental or reproductive phenotypes compared with wild-type rice. However, substantially low seed setting rates were observed when the *ago1d* mutants were grown in a paddy field at lower temperatures. We thus hypothesized that the *ago1d* mutants may have a temperature-sensitive fertility phenotype, because many photo/thermo-sensitive lines have recently been found to be related to the phasiRNA pathway. For example, *PMS1T*, a locus with a single-nucleotide polymorphism (SNP) producing 21-nt phasiRNAs, confers photosensitive male sterility in rice (Fan *et al.*, 2016), and the maize *dcl5* mutant, which loses the ability to generate 24-nt phasiRNAs, displays temperature-sensitive fertility (Teng *et al.*, 2020). Indeed, we further confirmed that *ago1d* mutants were male-sterile after being transferred to a glasshouse with an average temperature of 22°C at the panicle initiation stage. Cytological analysis showed that growing *ago1d* mutants at 22°C predominantly causes defects in tapetal PCD and pollen starch accumulation; by contrast, the meiotic defect rate was only slightly higher in the *ago1d* mutant compared with the wild-type. Thus, AGO1d is essential for anther development and pollen formation at lower temperatures in rice. It possible that AGO1d loading is more efficient than other AGO1 paralogs at low temperatures, such that there is redundancy at normal temperatures that is eliminated at low temperatures.

We showed by AGO1d RIP-seq data that AGO1d preferentially binds to *c.* 21-nt small RNAs with 5′ U, similar to the Arabidopsis AGO1 (Mi *et al.*, 2008). Moreover, except for 5′ U miRNAs, AGO1d also binds to 21-nt 5′ U phasiRNAs. Thus, in addition to MEL1 (OsAGO5c), which is known to prefer 21-nt phasiRNAs with 5′ C, we have identified AGO1d as an additional AGO that preferentially loads 21-nt phasiRNAs. Intriguingly, we found that AGO1d associates with both miR2118 and

miR2275, suggesting that AGO1d mediates the biogenesis of both 21- and 24-nt phasiRNAs. Small RNA sequencing data analysis has consistently revealed a substantial reduction in phasiRNAs from both 21- and 24-*PHAS* loci in the *ago1d* mutant. These results indicate that rice AGO1d mediates 21- and 24-nt phasiRNA biogenesis by forming RISCs with miR2118 and miR2275, respectively. Because the C-terminal fused tag may partially impair the slicing activity of the AGO protein (Yin *et al.*, 2020; Lee *et al.*, 2021), generating an endogenous AGO1d antibody would be helpful to confirm its binding preference and for additional experiments in the future. Notably, neither 21- or 24-nt phasiRNAs were completely eliminated in the *ago1d* mutant, suggesting that AGO1d may be functionally redundant with other AGO proteins, particularly AGO1a/b/c, considering the conservative cross-species preference of AGO1 for small RNAs with 5′ U (Fig. 6b). It is likely that at normal temperatures, functional redundancy is the main reason that *ago1d* mutants do not show fertility defects. By contrast, AGO1a/b/c activity might be decreased under lower temperatures so that they may not compensate for *ago1d* loss-of-function, leading to temperature-sensitive male sterility.

Like AGO1d, *AGO1b* mRNA expression shows anther wall specificity (Araki *et al.*, 2020), suggesting a potential functional redundancy with AGO1d. Indeed, CRISPR/Cas9-generated *ago1d ago1b* double mutant lines display partial male sterility at normal temperatures and full male sterility at lower temperatures (Fig. S13), supporting our hypothesis that AGO1 paralogs have functional redundancy in anther development and sterility maintenance. In a previous study (Wu *et al.*, 2009), AGO1a/b/c RIP-seq was performed using rice seedlings but not reproductive tissues. Thus, whether AGO1a/b/c paralogues play dual roles in phasiRNA biogenesis and function, similar to AGO1d, requires further investigation. Additional functional studies will be needed to establish the potential functional redundancy of all rice AGO1 paralogues during anther development.

Our analysis of transcriptome data demonstrated stage-specific dysregulation of crucial gene regulatory programs, such as transcriptional regulation, carbohydrate metabolism, and lipid transport and metabolism, which may confer *ago1d* sterility at lower temperatures. Notably, sugar and lipid metabolism-related genes have been widely reported to be crucial for pollen formation and male sterility (Wan *et al.*, 2020; Liu *et al.*, 2021). Using transcriptomic and metabolic profiling, we confirmed the disruption of metabolism in the *ago1d* mutant at lower temperatures. Thus, although AGO1d has a very mild impact on meiosis, it seems to control anther development and pollen formation at later stages through programming gene expression and cellular metabolism. Indeed, we confirmed the function of a phasiRNA in regulating sugar metabolism by negatively regulating the expression of a PFP that synthesizes D-fructose1,6-bisphosphate in glycolysis. Notably, only a small number of genes were identified as common phasiRNA targets between previous studies (Jiang *et al.*, 2020; Zhang *et al.*, 2020). Consistent with our analysis, a recent study also noted the discrepancies among previous studies of phasiRNA target identification and proposed that most of the genes reported in these studies might not be bona fide targets (Lan *et al.*, 2022). Thus, target validation of 21-nt phasiRNAs will likely rely on the development of novel techniques in the future. It is also possible that 21-nt phasiRNAs may play a role in translational repression, which may explain the difficulty of target identification by degradome sequencing.

Although the dysregulation of TEs was not observed in the *ago1d* mutant, there is evidence that phasiRNAs can repress TEs in germlines. A recent study reported that MAGO1 and MAGO2, two homologous proteins of rice MEL1 in maize, associate with temperature-induced 21-nt phasiRNAs to target TEs, safeguarding plant male fertility under high-temperature stress conditions (Lee *et al.*, 2021), suggesting roles of 21-nt phasiRNAs in transposon repression in addition to protein-coding gene silencing. A study in Arabidopsis demonstrated that tapetal 24-nt small RNAs can direct RdDM in germline cells (Long *et al.*, 2021). The biogenesis of 24-nt phasiRNA in the tapetum indicates that it may have a similar function during rice microsporogenesis (Fig. 6b), possibly by associating with AGO4a/b to mediate CHH DNA methylation (Zhang *et al.*, 2021). PhasiRNAs are not only found in monocots: they broadly exist with diversification in flowering plants (Xia *et al.*, 2019; Pokhrel *et al.*, 2021). We propose that an understanding of the mechanisms underlying reproductive phasiRNA biogenesis would facilitate precise artificial perturbation of phasiRNA pathways to generate novel photosensitive/thermosensitive sterile lines for hybrid breeding in a broader range of crops.

Acknowledgements

We thank members from the Fei Lab, Liang Lab, and Meyers Lab for helpful discussions. We thank Joanna Friesner for assistance in editing the text. This study was supported by the Guangdong Basic and Applied Basic Research Foundation (2019A1515110868), National Natural Science Foundation of China (32100289, U19A2031), and special funds for science technology innovation and industrial development of Shenzhen Dapeng New District (KJYF202001-01) to QF, and a US National Science Foundation award (no. 1754097) to BCM.

Author contributions

This project was conceived by QF, WL and BCM. Experiments were conducted by CS, JZ and CY. Data analyses were performed by BW, CS, RJ and QF. The manuscript was written by CS and QF with input from all authors. CS and JZ contributed equally to this work.

ORCID

Qili Fei https://orcid.org/0000-0002-0860-2175
Wanqi Liang https://orcid.org/0000-0002-9938-5793
Blake C. Meyers https://orcid.org/0000-0003-3436-6097
Chuanlin Shi https://orcid.org/0000-0003-4776-1942
Jie Zhang https://orcid.org/0000-0003-4725-8407

Data availability

Raw small RNA and transcriptome sequencing data generated in this study are available at Gene Expression Omnibus (GEO), under GSE191268. Other data generated during this study are included in this published article and the accompanying Supporting Information files.

References

Araki S, Le NT, Koizumi K, Villar-Briones A, Nonomura KI, Endo M, Inoue H, Saze H, Komiya R. 2020. miR2118-dependent U-rich phasiRNA production in rice anther wall development. *Nature Communications* **11**: 3115.

Bologna NG, Iselin R, Abriata LA, Sarazin A, Pumplin N, Jay F, Grentzinger T, Dal Peraro M, Voinnet O. 2018. Nucleo-cytosolic shuttling of ARGONAUTE1 prompts a revised model of the plant microRNA pathway. *Molecular Cell* **69**: 709–719.

Borges F, Martienssen RA. 2015. The expanding world of small RNAs in plants. *Nature Reviews. Molecular Cell Biology* **16**: 727–741.

Chen C, Chen H, Zhang Y, Thomas HR, Frank MH, He Y, Xia R. 2020. TBtools: an integrative toolkit developed for interactive analyses of big biological data. *Molecular Plant* **13**: 1194–1202.

Chen HM, Chen LT, Patel K, Li YH, Baulcombe DC, Wu SH. 2010. 22-nucleotide RNAs trigger secondary siRNA biogenesis in plants. *Proceedings of the National Academy of Sciences, USA* **107**: 15269–15274.

Cuperus JT, Carbonell A, Fahlgren N, Garcia-Ruiz H, Burke RT, Takeda A, Sullivan CM, Gilbert SD, Montgomery TA, Carrington JC. 2010. Unique functionality of 22-nt miRNAs in triggering RDR6-dependent siRNA biogenesis from target transcripts in *Arabidopsis*. *Nature Structural & Molecular Biology* **17**: 997–1003.

Derrien B, Baumberger N, Schepetilnikov M, Viotti C, De Cillia J, Ziegler-Graff V, Isono E, Schumacher K, Genschik P. 2012. Degradation of the antiviral component ARGONAUTE1 by the autophagy pathway. *Proceedings of the National Academy, USA* **109**: 15942–15946.

Fan Y, Yang J, Mathioni SM, Yu J, Shen J, Yang X, Wang L, Zhang Q, Cai Z, Xu C *et al.* 2016. PMS1T, producing phased small-interfering RNAs, regulates photoperiod-sensitive male sterility in rice. *Proceedings of the National Academy of Sciences, USA* **113**: 15144–15149.

Fei Q, Xia R, Meyers BC. 2013. Phased, secondary, small interfering RNAs in posttranscriptional regulatory networks. *Plant Cell* **25**: 2400–2415.

Fei Q, Yang L, Liang W, Zhang D, Meyers BC. 2016. Dynamic changes of small RNAs in rice spikelet development reveal specialized reproductive phasiRNA pathways. *Journal of Experimental Botany* **67**: 6037–6049.

Fei Q, Yu Y, Liu L, Zhang Y, Baldrich P, Dai Q, Chen X, Meyers BC. 2018. Biogenesis of a 22-nt microRNA in Phaseoleae species by precursor-programmed uridylation. *Proceedings of the National Academy of Sciences, USA* **115**: 8037–8042.

Hirose T, Zhang ZJ, Miyao A, Hirochika H, Ohsugi R, Terao T. 2010. Disruption of a gene for rice sucrose transporter, OsSUT1, impairs pollen function but pollen maturation is unaffected. *Journal of Experimental Botany* **61**: 3639–3646.

Jiang P, Lian B, Liu C, Fu Z, Shen Y, Cheng Z, Qi Y. 2020. 21-nt phasiRNAs direct target mRNA cleavage in rice male germ cells. *Nature Communications* **11**: 5191.

Johnson C, Kasprzewska A, Tennessen K, Fernandes J, Nan GL, Walbot V, Sundaresan V, Vance V, Bowman LH. 2009. Clusters and superclusters of phased small RNAs in the developing inflorescence of rice. *Genome Research* **19**: 1429–1440.

Kawahara Y, de la Bastide M, Hamilton JP, Kanamori H, McCombie WR, Ouyang S, Schwartz DC, Tanaka T, Wu J, Zhou S *et al.* 2013. Improvement of the Oryza sativa Nipponbare reference genome using next generation sequence and optical map data. *Rice* **6**: 4.

Kim D, Paggi JM, Park C, Bennett C, Salzberg SL. 2019. Graph-based genome alignment and genotyping with HISAT2 and HISAT-genotype. *Nature Biotechnology* **37**: 907–915.

Komiya R, Ohyanagi H, Niihama M, Watanabe T, Nakano M, Kurata N, Nonomura K. 2014. Rice germline-specific Argonaute MEL1 protein binds to phasiRNAs generated from more than 700 lincRNAs. *The Plant Journal* **78**: 385–397.

Kozomara A, Birgaoanu M, Griffiths-Jones S. 2019. miRBase: from microRNA sequences to function. *Nucleic Acids Research* **47**: D155–D162.

Lan T, Yang X, Chen J, Tian P, Shi L, Yu Y, Liu L, Gao L, Mo B, Chen X *et al.* 2022. Mechanism for the genomic and functional evolution of the MIR2118 family in the grass lineage. *The New Phytologist* **233**: 1915–1930.

Langmead B, Trapnell C, Pop M, Salzberg SL. 2009. Ultrafast and memory-efficient alignment of short DNA sequences to the human genome. *Genome Biology* **10**: R25.

Lee YS, Maple R, Durr J, Dawson A, Tamim S, Del Genio C, Papareddy R, Luo A, Lamb JC, Amantia S *et al.* 2021. A transposon surveillance mechanism that safeguards plant male fertility during stress. *Nature Plants* **7**: 34–41.

Li C, Zhang B. 2016. MicroRNAs in control of plant development. *Journal of Cellular Physiology* **231**: 303–313.

Li S, Liu L, Zhuang X, Yu Y, Liu X, Cui X, Ji L, Pan Z, Cao X, Mo B *et al.* 2013. MicroRNAs inhibit the translation of target mRNAs on the endoplasmic reticulum in Arabidopsis. *Cell* **153**: 562–574.

Liao Y, Smyth GK, Shi W. 2014. featureCounts: an efficient general purpose program for assigning sequence reads to genomic features. *Bioinformatics* **30**: 923–930.

Lim H, Cho MH, Jeon JS, Bhoo SH, Kwon YK, Hahn TR. 2009. Altered expression of pyrophosphate: fructose-6-phosphate 1-phosphotransferase affects the growth of transgenic Arabidopsis plants. *Molecules and Cells* **27**: 641–649.

Liu C, Xin Y, Xu L, Cai Z, Xue Y, Liu Y, Xie D, Liu Y, Qi Y. 2018. Arabidopsis ARGONAUTE 1 binds chromatin to promote gene transcription in response to hormones and stresses. *Developmental Cell* **44**: 348–361.

Liu SS, Li ZW, Wu SW, Wan XY. 2021. The essential roles of sugar metabolism for pollen development and male fertility in plants. *Crop Journal* **9**: 1223–1236.

Liu Y, Teng C, Xia R, Meyers BC. 2020. PhasiRNAs in plants: their biogenesis, genic sources, and roles in stress responses, development, and reproduction. *Plant Cell* **32**: 3059–3080.

Long J, Walker J, She W, Aldridge B, Gao H, Deans S, Vickers M, Feng X. 2021. Nurse cell-derived small RNAs define paternal epigenetic inheritance inArabidopsis. *Science* **373**: eabh0556.

Ma X, Zhang Q, Zhu Q, Liu W, Chen Y, Qiu R, Wang B, Yang Z, Li H, Lin Y *et al.* 2015. A robust CRISPR/Cas9 system for convenient, high-efficiency multiplex genome editing in monocot and dicot plants. *Molecular Plant* **8**: 1274–1284.

Mi S, Cai T, Hu Y, Chen Y, Hodges E, Ni F, Wu L, Li S, Zhou H, Long C *et al.* 2008. Sorting of small RNAs into Arabidopsis argonaute complexes is directed by the 5′ terminal nucleotide. *Cell* **133**: 116–127.

Nonomura K, Morohoshi A, Nakano M, Eiguchi M, Miyao A, Hirochika H, Kurata N. 2007. A germ cell specific gene of the ARGONAUTE family is essential for the progression of premeiotic mitosis and meiosis during sporogenesis in rice. *Plant Cell* **19**: 2583–2594.

Ono S, Liu H, Tsuda K, Fukai E, Tanaka K, Sasaki T, Nonomura KI. 2018. EAT1 transcription factor, a non-cell-autonomous regulator of pollen production, activates meiotic small RNA biogenesis in rice anther tapetum. *PLoS Genetics* **14**: e1007238.

Ouyang S, Buell CR. 2004. The TIGR plant repeat databases: a collective resource for the identification of repetitive sequences in plants. *Nucleic Acids Research* **32**: D360–D363.

Petrov AI, Kay SJE, Kalvari I, Howe KL, Gray KA, Bruford EA, Kersey PJ, Cochrane G, Finn RD, Bateman A *et al.* 2017. RNAcentral: a comprehensive database of non-coding RNA sequences. *Nucleic Acids Research* **45**(D1): D128–D134.

Plaxton WC. 1996. The organization and regulation of plant glycolysis. *Annual Review of Plant Physiology and Plant Molecular Biology* **47**: 185–214.

Pokhrel S, Huang K, Belanger S, Zhan J, Caplan JL, Kramer EM, Meyers BC. 2021. Pre-meiotic 21-nucleotide reproductive phasiRNAs emerged in seed plants and diversified in flowering plants. *Nature Communications* **12**: 4941.

Song L, Fang Y, Chen L, Wang J, Chen X. 2021. Role of non-coding RNAs in plant immunity. *Plant Communication* **2**: 100180.

Song X, Li P, Zhai J, Zhou M, Ma L, Liu B, Jeong DH, Nakano M, Cao S, Liu C *et al.* 2012. Roles of DCL4 and DCL3b in rice phased small RNA biogenesis. *The Plant Journal* **69**: 462–474.

Song X, Li Y, Cao X, Qi Y. 2019. MicroRNAs and their regulatory roles in plant–environment interactions. *Annual Review of Plant Biology* **70**: 489–525.

Teng C, Zhang H, Hammond R, Huang K, Meyers BC, Walbot V. 2020. Dicer-like 5 deficiency confers temperature-sensitive male sterility in maize. *Nature Communications* **11**: 2912.

Tian T, Liu Y, Yan H, You Q, Yi X, Du Z, Xu W, Su Z. 2017. AGRIGO v.2.0: a GO analysis toolkit for the agricultural community, 2017 update. *Nucleic Acids Research* **45**(W1): W122–W129.

Trapnell C, Williams BA, Pertea G, Mortazavi A, Kwan G, van Baren MJ, Salzberg SL, Wold BJ, Pachter L. 2010. Transcript assembly and quantification by RNA-Seq reveals unannotated transcripts and isoform switching during cell differentiation. *Nature Biotechnology* **28**: 511–515.

Wan X, Wu S, Li Z, An X, Tian Y. 2020. Lipid metabolism: critical roles in male fertility and other aspects of reproductive development in plants. *Molecular Plant* **13**: 955–983.

Wang H, Hu Q, Tang D, Liu X, Du G, Shen Y, Li Y, Cheng Z. 2016. OsDMC1 is not required for homologous pairing in rice meiosis. *Plant Physiology* **171**: 230–241.

Wu L, Zhang Q, Zhou H, Ni F, Wu X, Qi Y. 2009. Rice MicroRNA effector complexes and targets. *Plant Cell* **21**: 3421–3435.

Xia R, Chen C, Pokhrel S, Ma W, Huang K, Patel P, Wang F, Xu J, Liu Z, Li J *et al.* 2019. 24-nt reproductive phasiRNAs are broadly present in angiosperms. *Nature Communications* **10**: 627.

Yin W, Xiao Y, Niu M, Meng W, Li L, Zhang X, Liu D, Zhang G, Qian Y, Sun Z *et al.* 2020. ARGONAUTE2 enhances grain length and salt tolerance by activating BIG GRAIN3 to modulate cytokinin distribution in rice. *Plant Cell* **32**: 2292–2306.

Yoshikawa M, Han YW, Fujii H, Aizawa S, Nishino T, Ishikawa M. 2021. Cooperative recruitment of RDR6 by SGS3 and SDE5 during small interfering RNA amplification in Arabidopsis. *Proceedings of the National Academy of Sciences, USA* **118**: e2102885118.

Yu B, Liu LT, Wang T. 2019. Deficiency of very long chain alkanes biosynthesis causes humidity-sensitive male sterility via affecting pollen adhesion and hydration in rice. *Plant, Cell & Environment* **42**: 3340–3354.

Zhai J, Jeong DH, De Paoli E, Park S, Rosen BD, Li Y, Gonzalez AJ, Yan Z, Kitto SL, Grusak MA *et al.* 2011. MicroRNAs as master regulators of the plant *NB-LRR* defense gene family via the production of phased, *trans*-acting siRNAs. *Genes & Development* **25**: 2540–2553.

Zhai J, Zhang H, Arikit S, Huang K, Nan G, Walbot V, Meyers BC. 2015. Spatiotemporally dynamic, cell-type-dependent premeiotic and meiotic phasiRNAs in maize anthers. *Proceedings of the National Academy of Sciences, USA* **112**: 3146–3151.

Zhang D, Luo X, Zhu L. 2011. Cytological analysis and genetic control of rice anther development. *Journal of Genetics and Genomics* **38**: 379–390.

Zhang H, Xia R, Meyers BC, Walbot V. 2015. Evolution, functions, and mysteries of plant ARGONAUTE proteins. *Current Opinion in Plant Biology* **27**: 84–90.

Zhang M, Ma X, Wang C, Li Q, Meyers BC, Springer NM, Walbot V. 2021. CHH DNA methylation increases at 24-PHAS loci depend on 24-nt phased small interfering RNAs in maize meiotic anthers. *The New Phytologist* **229**: 2984–2997.

Zhang Y, Su J, Duan S, Ao Y, Dai J, Liu J, Wang P, Li Y, Liu B, Feng D *et al.* 2011. A highly efficient rice green tissue protoplast system for transient gene expression and studying light/chloroplast-related processes. *Plant Methods* **7**: 30.

Zhang YC, Lei MQ, Zhou YF, Yang YW, Lian JP, Yu Y, Feng YZ, Zhou KR, He RR, He H *et al.* 2020. Reproductive phasiRNAs regulate reprogramming of gene expression and meiotic progression in rice. *Nature Communications* **11**: 6031.

Zhao J, Long T, Wang Y, Tong X, Tang J, Li J, Wang H, Tang L, Li Z, Shu Y *et al.* 2020. RMS2 encoding a GDSL lipase mediates lipid homeostasis in anthers to determine rice male fertility. *Plant Physiology* **182**: 2047–2064.

Supporting Information

Additional Supporting Information may be found online in the Supporting Information section at the end of the article.

Dataset S1 miRNA abundances (reads per million) in the RNA immunoprecipitation sequencing data.

Dataset S2 21-/24-nt phasiRNA abundances (reads per million) from the *PHAS* loci in the small RNA-seq data.

Dataset S3 miRNA abundances (reads per million) in the small RNA-seq data.

Dataset S4 Differentially expressed genes and the abundances (fragments per kilobase of transcript per million mapped reads) in the transcriptome data at rice anther developmental stage 4–6, 7–8 and 9.

Dataset S5 Relative content of metabolites in mass spectrometry.

Fig. S1 Tissue specificity and subcellular localization of all four rice AGO1s.

Fig. S2 The male fertility phenotypes of the *ago1d* mutant.

Fig. S3 Chromosome behaviors of wild-type and *ago1d* male meiocytes at 22°C.

Fig. S4 Western blots and RIP-seq using a *pAGO1d::AGO1d-FLAG* transgenic line.

Fig. S5 Enrichment of small RNAs in the AGO1d-FLAG RIP-seq data.

Fig. S6 PhasiRNA and miRNA abundances in wild-type and *ago1d* anthers.

Fig. S7 Expression levels (fragments per kilobase of transcript per million mapped reads) of *AGO1d* paralogous genes in wild-type and *ago1d* anthers grown at either 28°C or 22°C.

Fig. S8 Expression levels (fragments per kilobase of transcript per million mapped reads) of additional genes known to function in the regulation of anther development from overlapped differentially expressed gene lists.

Fig. S9 Expression levels (fragments per kilobase of transcript per million mapped reads) of genes enriched in carbohydrate metabolic processes and glycosyltransferase activity from overlapped differentially expressed gene lists.

Fig. S10 Expression levels (fragments per kilobase of transcript per million mapped reads) of genes enriched in lipid transport, localization and metabolism processes from overlapped differentially expressed gene lists.

Fig. S11 Mass spectrometry analysis of metabolites in the anthers of wild-type and *ago1d* S9 plants grown at either 28°C or 22°C.

Fig. S12 Analysis of 21-nt phasiRNA targets from two published datasets in the anthers of wild-type and *ago1d* mutant plants grown at either 28°C or 22°C.

Fig. S13 The male-sterile phenotypes of the *ago1d ago1b* double mutant.

Table S1 A list of primers used in this study.

Table S2 Abundances (reads per million) of different members of miR2118 in the RIP-seq data.

Table S3 Members of miR2275 in the rice genome.

Table S4 Abundances (reads per million) of different members of miR2275 in the RIP-seq data.

Please note: Wiley Blackwell are not responsible for the content or functionality of any Supporting Information supplied by the authors. Any queries (other than missing material) should be directed to the *New Phytologist* Central Office.